European volcanological supersite in Iceland: a monitoring system and network for the future

Report

D6.5 MT Solutions and Modelling of Tremor

Work Package:	*Imminent eruptive activity, eruption onset and early warning*
Work Package number:	*6*
Deliverable:	*MT solutions and modelling of Tremor*
Deliverable number:	*6.5*
Type of Activity:	*RTD*
Responsible activity leader:	*K. S. Vogfjörd*
Responsible participant:	*IMO*
Authors:	*Eva Eibl (UCD), Johannes Thun (UCD), Christopher Bean (UCD), Yingzi Ying (UCD), Kristin S. Vogfjörd (IMO)*

Type of Deliverable:	*Report*	*[×]*	*Demonstrator*	*[ ]*
	Prototype	*[ ]*	*Other*	*[ ]*
Dissemination level:	*Public*	*[x]*	*Restricted Designated Group*	*[ ]*
	Prog. Participants (FP7)	*[ ]*	*Confidential (consortium)*	*[ ]*

Seventh Framework Programme
EC project number: 308377

Introduction

The precise causes of seismic tremor are poorly understood although tremor signals have been associated with a variety of processes on glacier covered volcanoes, including: magma flow, sub-glacial flooding and hydrothermal boiling (see Deliverable D6.3). Long Period (LP) seismic events are often intimately associated with pre-eruptive activity, especially on andesitic volcanoes – and swarms of LP events often merge into continuous seismic tremor. At the concept phase of FutureVolc we intended to study this phenomenon, but it transpired that very few LP events were detected. Our original aim was to apply Moment Tensor (MT) solutions to LP events in an effort to better understand tremor. Moment Tensor solutions give not only the 'focal mechanism' of the source, but also the source time history, allowing for a more complete description of the seismic source. The lack of LP detections is almost certainly partly related to the geological environment but might also be related to insufficient detection as the planned bespoke glacier seismometers were delayed due to technical reasons. Hence given that our primary objective in this deliverable (D6.5) is to better understand seismic sources associated with magmatic processes/dyke formation, we opt to take a different approach to this problem which we believe has yielded a deeper understanding of process than traditional MT solution might have brought. This deliverable should be read in association with D6.3, which gives some of the background to tremor analysis and tremor in the region. D6.3 was a phenomenological approach, that is we looked at processes and identified what tremor signals those processes generated. Whilst the results of this approach can be used in practice in terms for eruption forecasting, it does not necessarily give a deep understanding of precisely why tremor is being generated and hence does not reveal the details of the source process. Therefore here in D6.5 we do two things (1) look for an understanding of the processes that can generate tremor, with a focus on 'magmatic' tremor (2) look directly at the seismic source using specially deployed 'on-dyke' (nearfield) seismic observations of dyke opening immediately North of Vatnajökull, during the Holuhraun eruption. By applying a novel processing method to the nearfield seismic data (Thun et al, 2015), we are able use the seismometer as a displacement instrument. We can resolve displacements down to a few microns with this method. Hence it gives us an unprecedented look at the source process – that is, how the dyke is opening at micrometre spatial scale and millisecond temporal scale.

Source versus Path effects

Seismic waves are distorted as they propagate through the Earth. For a given propagation distance, this distortion is more pronounced for high frequency waves as they have more seismic 'cycles' per unit distance. For fault plane solution calculations which are based on the polarities of the first seismic picks, moderate levels of distortion can be tolerated. However for methods that involve waveform fits (that is fitting synthetic waveforms to observed waveforms) the path effects need to be estimated and removed because waveform shapes are sensitive to the paths through which the 'waveform' travels. In volcano work where there is often a lack of events with a sufficient range of magnitudes to take the empirical Green's function approach (that is, using a small events to estimate the paths effects for a larger event of interest, at the same location), numerical simulations are used to estimate and remove path effects (e.g. Bean et al, 2008). This requires that we obtain an acceptable seismic velocity model for the area of interest so that path effects can be numerically simulated. The situation is the same with seismic tremor in terms of path effect distortions. On glacier covered volcanoes seismomters are usually placed around the edges of the ice and potentially on nunataks. The signal that is recorded is therefore not only affected by the path the wave travelled in the bedrock but is potentially trapped in the ice or the low velocity layer just below the rock-ice interace

Seismic tremor sources are 'continuous' in time and quasi-static in space, when compared to seismic wave propagation velocities. Hence, if we imagine a 'tremor wavelet' (a small 'slice' of tremor) at any point in time, that wavelet will be distorted by path effects as it travels. However a continuous tremor recording comprises multiple 'repeating' wavelets all superimposed with some time delay. Hence when we look at the whole recorded tremor signal, the source and path effects are all intertwined and we cannot distinguish one from the other. Here we combine this 'tremor wavelet' idea with the need to remove path effects (as outline above) to model synthetic tremor for comparison with real observed tremor at Vatnajökull. As mentioned above, the situation at Vatnajökull is particularly complex as the numerical calculations to estimate path effect must also take into account the wave propagation effects of the glacial ice. Hence the first task is to construct a velocity model of the region, which includes the ice layer, basal and top surface ice topography and the sub-surface geology. Building a full 3D model from raw seismic data using tomography, for example, is beyond the scope of this deliverable. Hence our approach is to focus on the geometry of the ice from radar observations and to construct the subsurface geological/seismic velocity model, based on existing models in the published literature.

Constructing the velocity model: Our model for tremor simulations encompasses a region that includes Vatna Glacier (see Figure 6.5.2). Ice surface and bedrock topography based on radar measurements were provided by Finnur Pálsson of the University of Iceland. We derived an average 1D velocity model for the volcanic region around western Vatnajokull glacier from the full range of published velocity-depth curves available in the literature (figure 6.5.1; see reference in the figure caption). A seismic P-wave velocities of 3.8 km/s in temperate ice is used, also based on published work. As can be seen in figure 6.5.2 the model extends beyond the ice-field, and also includes land surface topopgraphy in that region. Hence, the model is 2-dimensional in terms of land-surface, ice-surface and ice-basal topography, but 1-dimemsional in seismic velocity in the sub-surface. This is the most complete model that we were able to construct at this point in time. The surface topographies are included, as surfaces are known to be strong scatterers of seismic waves (e.g. Bean & Martini, 2010). There are a few things to note about this velocity model (i) there is a strong velocity gradient in the upper 2km, which will act as a wave-guide (ii) the velocity-depth curves were largely derived from regional refraction seismic surveys, hence the near-surface (*c.* top 500m) is not properly sampled in those experiments – hence, based on our previous work in other localities we suspect that the near surface velocity is too high in the model in figure 6.5.2. (iii) despite the previous point about the high near-surface velocities, there is still a significant velocity inverion beneath the ice. This Low Velocity Zone (LVZ) will trap waves, especially for seismic signals generated in or close to the LVZ itself.

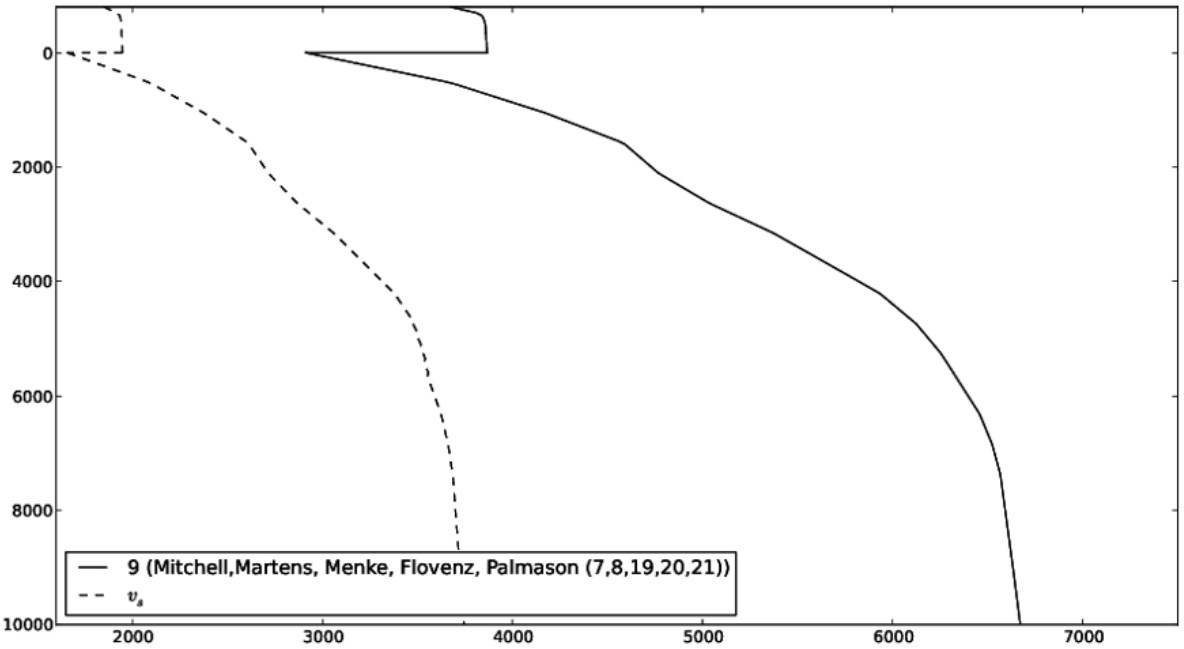

Figure 6.5.1: Velocity models of Mitchell2013, Martens2010, Menke1995 and Palmason1963 averaged (solid black line). Vs is derived using a Poisson ratio of 0.26 in the upper crust and 0.27 in the lower crust as published in Darbyshire1998 and Palmason1963. X-axis is velocity (km/s). Y-axis is depth (m)

Numerical simulation of seismic wave propagation effects are undertaken using SPECFEM3D, which is a full wavefield simulator. In figure 6.5.2 we show seismograms from one of our simulations. The star in figure 6.5.3 marks the location of the source, the triangle the location of the seismometer. Although the seismic source is only a 1 Hz Ricker wavelet of a few seconds duration, the seismogram recorded at 50 km distance is about 40 s long. Hence, in the physical world, if we imagine that a small `slice` of tremor <u>at its source</u> is extracted and represented by our 1Hz (*c*. 3 sec long) Ricker wavelet pulse, then this modelling shows us that that piece of the `tremor source` will appear at our seismic station as a *c.* 40 second long seismic arrival (even though it was only 3 sec long at the source). It follows that the next adjacent `slice` of 3 sec long tremor at the source will also be 40 seconds long at the station and will over lap the original slice by > 90% or their trace lengths.

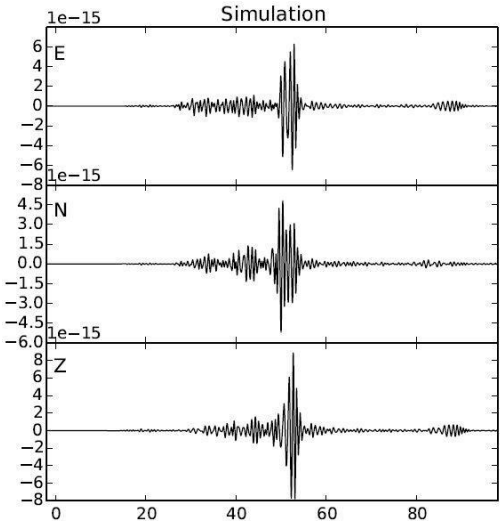

Figure 6.5.2 Numerical synthetic seismograms
From a 1Hz Ricker wavelet recorded at 50 km distance
(see Figure 6.5.2 for source and station locations). X-axis is time (s)

If we repeat this process multiple times we see that the recorded data stream at the seismometer will be markedly different to the actual tremor that is being generated at its source. Hence if we are several 10s of km from the tremor source, as is commonly the case in Iceland in the pre-eruptive phase of a crisis, there is little obvious relationship between the details of the recorded tremor and the details of the source process. Hence

it is difficult to quantify the source physically, based on the far-field tremor signal alone (note: however we can quantify it phenomenologically, based on the arguments in deliverable D6.3), unless we have a clear *apriori* model for tremor generation, at its source. We will formalise this tremor generation idea in the next section below, hypothesizing a source model and using it to generate synthetic tremor signals for comparison with real data.
Figure 6.5.3 also shows the seismic wavefield sensitivity kernels. Sensitivity kernels highlight the parts of the seismic velocity model that most influence the seismograms. That is, they highlight the parts of the models to which the seismograms are most sensitive.

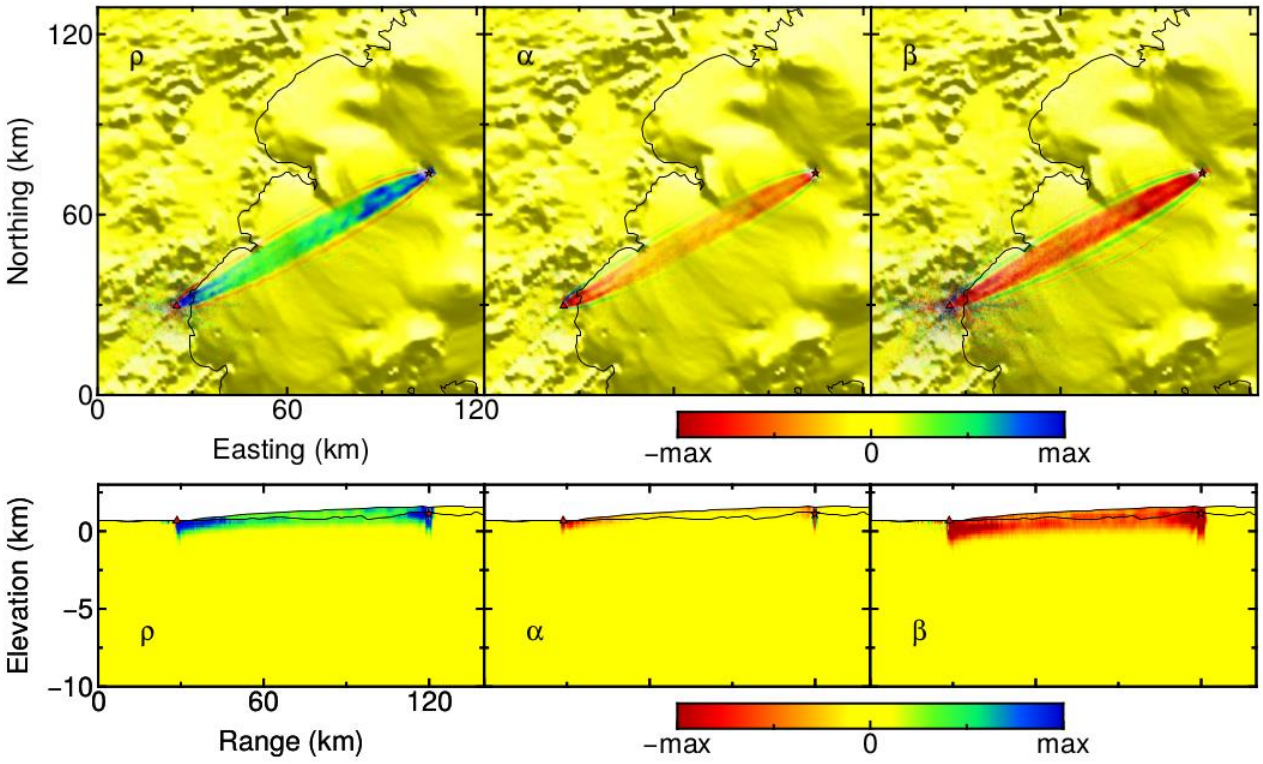

Figure 6.5.3: Top row: Map view of the kernels on the surface and source (star) and station (triangle) locations - western edge of the glacier is indiacted by the black line. Bottom row: Cross section view of sensitivities. In both panels sensitivity of P waves (alpha), S waves (beta) and density (rho) to different regions of the model are given.

As is clear in the cross sections in figure 6.5.3, the LVZ at the base of the ice is acting as a very significant wave guide for tremor originating at the rock-ice interface. Also, sensitivity to P-waves is weak, and is stronger for density and S-wave velocity, demonstrating that the recorded waveform primarily comprises S and Surface waves.

Physical model for tremor source generation

In the preceding section we introduced the concept of a repeating source playing a role in tremor generation. This idea has been put forward before. Long Period (LP) events are often seen to merge into tremor and strong tremor frequency gliding associated with the 2009 eruption of Redoubt volcano in Alaska was modelled as rapidly repeating events (Hotovec et al, 2013). The tremor that we have detected that is likely associated with magma movement is harmonic (see example in figure 6.5.4).

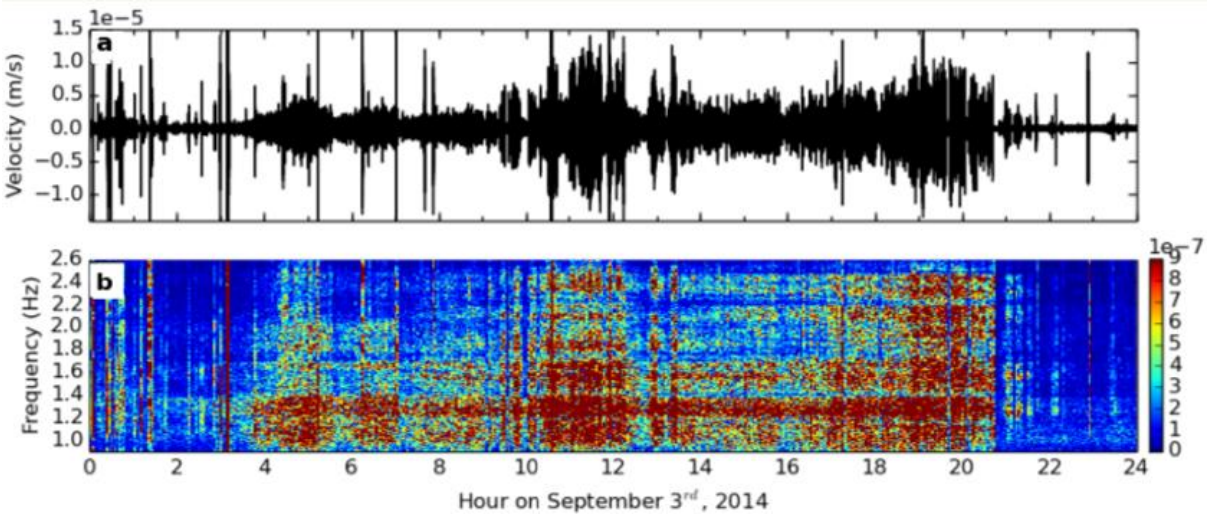

Figure 6.5.5 (a) Seismogram from station UR (see deliverable 6.3), filtered between 0.9-2.6 Hz on September 3rd, 2014. (b) Spectrogram of (a) above.

Here we model this tremor as a sequence of rapidly repeating pulse-like (Ricker wavelet) events of different amplitudes. Having run a suite of trials we chose repeat times for the events that are almost regular, but with 10% random noise on their timings. The amplitude distribution of the events is power-law.
Although we envision a repeating pulse at the source, the ensuing wavelet propagates to our seismic station and is distorted (in our case the station is *c*. 50km from the source). Hence it is the vertical component synthetic seismogram in figure 6.2.5 that we actually use as our quasi-regular repeating pulse. We are also able to simulate tremor from different depths, using a full wavefield simulation with a source at the required depth in order to generate the 'core' seismogram.
A comparison between real and synthetic tremor is given in figure 6.5.6. It is clear from this comparison that this approach generates synthetic tremor that is at least visually strikingly similar to real magma related tremor signals.
We can conclude from this finding that a processes that involves repeat 'pulsing' at the source, can generate synthetic tremor signals that are visually indistinguishable from real tremor.

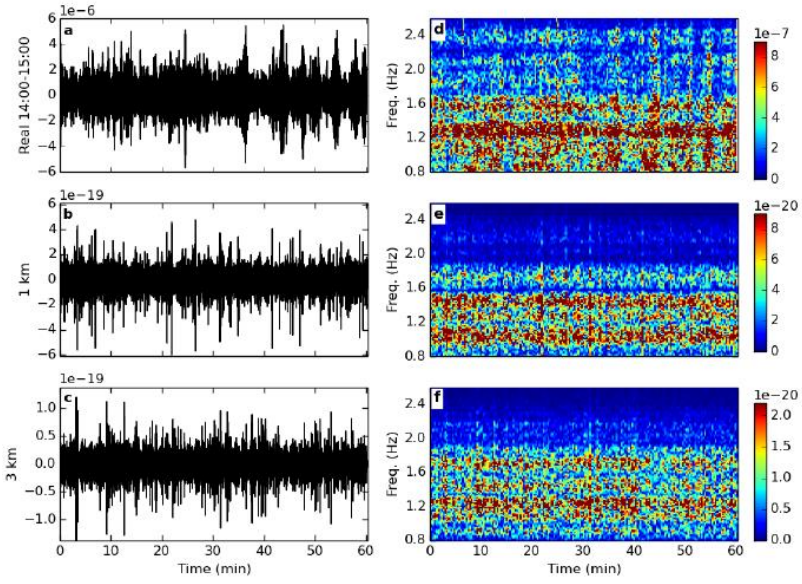

Figure 6.5.6
(a) & (d), real tremor and its spectrogram
(b) & (e), synthetic tremor generated as described in the text and it spectrogram – source at 1km depth
(c) & (f), synthetic tremor and its spectrogram – source at 3km depth

Very near dyke field observation & source inversion

As outline above, we have taken advantage of the Holuhraun eruption to look at source processes more directly than is possible with far-field seismic observations. This also allows us to mitigate the lack of Long Period (LP) events on which we had hoped to perform Moment Tensor (MT) solutions. With the near-field observations outlined below, we negate the need for MT inversion on dynamic seismograms as we can obtain significant information directly about the source from static displacements on seismometer data. This has the advantage of very low sensitivity to material heterogeneity relative to higher frequency dynamic seismic waves.
The pre-existing Holuhraun eruptive fissure, located approximately 5 – 10 km North of the Vatnajökull glacier, erupted for 4 hours on 29th August 2014 and then for 6 months starting 31th August. In the afternoon of 30th August 2014 we installed a small profile of three 3-component broadband seismometers (Guralp 6TD 30 s) perpendicular to the graben and inferred dyke (Figure 6.5.7A), with the closest station (DY3) directly at the shoulder of a large surface fracture and the other two stations approximately 1 km (DY1) and 2 km (DY2) away. As strong ground shaking could be felt during the experiment, it had to be aborted for safety reasons, resulting in only ~26 minutes of synchronous data on all stations. Eventually, a new fissure opened as close as 600 m east of DY3 and effused lava for 2 days from 5th September 2014.

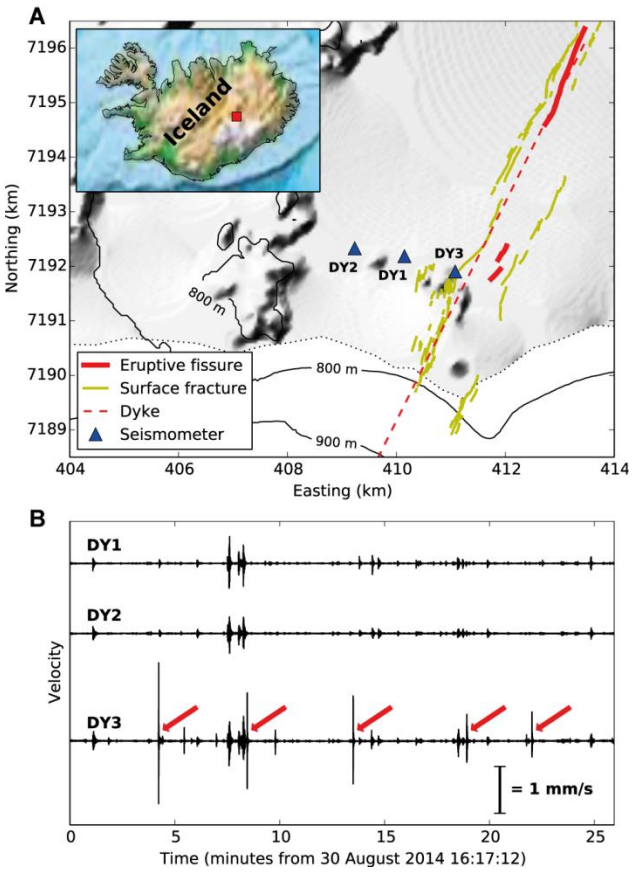

Figure 6.5.7: Overview of seismic experiment and recorded data. A: Map of stations DY1, DY2 and DY3 (Guralp 6TD (30s) seismometers) installed north of the Vatnajökull glacier (white) on 30 August 2014 in direct vicinity of several large surface fractures; inset map shows the location within Iceland. Eruptive fissures and fractures mapped by Hjartardóttir et al. (2016); dyke location from Sigmundsson et al. (2015); elevation data from National Land Survey of Iceland. B: Unfiltered vertical recordings on all three stations. Arrows mark the step events on DY3 investigated in this study. These events are not visible on stations DY1 and DY2.

The unprocessed vertical velocity seismograms (Fig. 6.5.7B) show a lot of coherent activity on all three stations, presumably activity from the dyke area, although only three of the events appear in the earthquake catalogue from the Icelandic Met Office (pers. comm. K. S. Vogfjord, October 2015). However, the focus of this study lies on five strong events on station DY3 (marked by red arrows in Fig. 6.5.7B), which are not registered by the other two instruments, suggesting that they are (dynamically) small and local to station DY3.
The velocity seismograms and the corresponding scalograms of these events (e.g. event number 3 in Fig. 6.5.8) show impulsive waveforms with a main frequency peak between 3 and 8 Hz and a secondary peak above 25 Hz. In a recent study (Thun et al., 2015), we presented a new approach to long-period noise removal from instrument-corrected seismograms. This allows a recovery of small displacement steps with short rise times from the data and was shown to yield good results for laboratory data. We apply this processing to the events at DY3 (3 bottom panels in Fig. 6.5.8) and observe displacement steps on all three components, i.e. the station was displaced by approximately 125 µm in northwest, slightly upward direction.

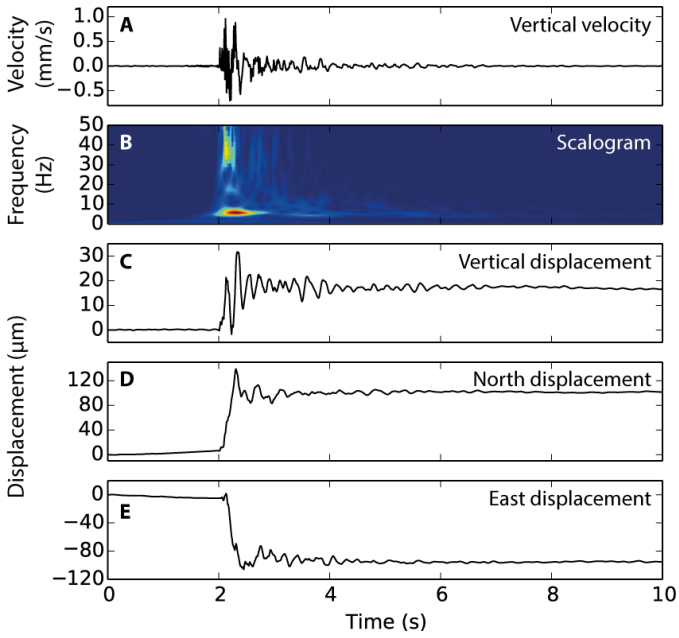

Figure 6.5.8: Third step event recorded by station GLDY3. A: Vertical velocity waveform (instrument corrected); B: corresponding velocity scalogram illustrating relative frequency content – the main frequency peak of the events lies between 3 Hz and 8 Hz, with an additional peak above 25 Hz. C-E: Vertical, North and East displacements, respectively; these have been processed with the median filter method presented in Thun et al. (2015). Recovered displacement steps are about 17 µm upward and 123 µm in North-West direction.

This represents a motion away from the graben and the underlying dyke. Applying this procedure to all three full-length seismograms on this station (Fig. 6.5.9A) reveals similar amplitudes and ratios between different displacement components for all five events, suggesting a repetitive process with similar source locations and magnitudes. As horizontal components of seismometers are also susceptible to ground rotation, possible tilts can be estimated from the data using the tilt transfer function (e.g. Lyons et al.

2012). The resulting traces (Fig. 6.5.9B) show tilt steps of 1.3 – 4 µrad oriented in a northwest direction associated with each of the five events. The long-period trend is likely instrumental noise and cannot be interpreted directly. The tilt step directions are in excellent agreement with the direction of the displacement steps and corroborate a repeating source process between the events (Fig. 6.5.9C) with roughly consistent step amplitudes and locations.

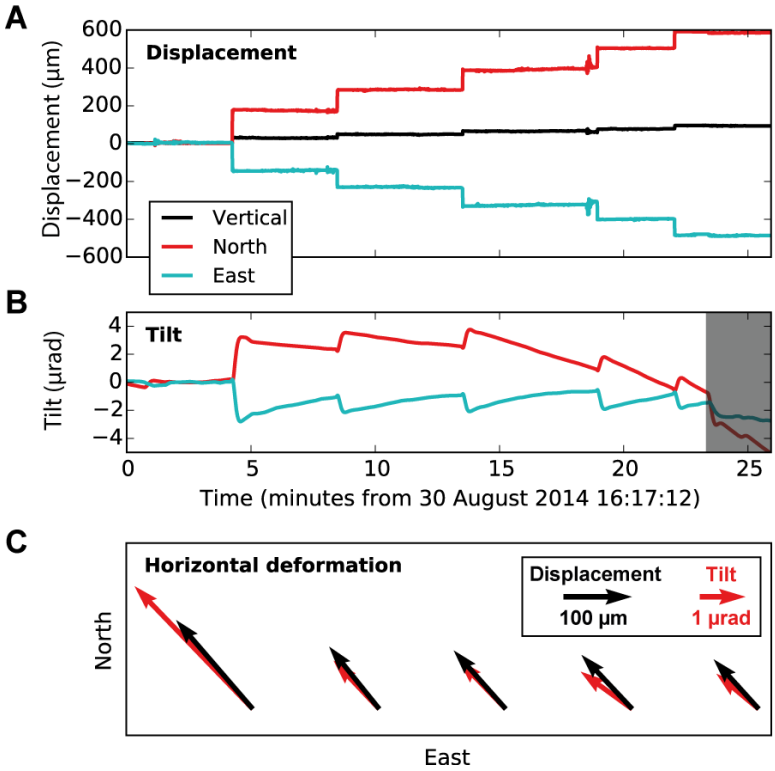

Figure 6.5.9: Full-length seismograms processed to show ground deformation. A: Median filter processed for step recovery (black: Vertical, red: North, cyan: East), showing a consistency of step direction between the events. Note that between events 3 and 4, a longer period event impedes the filter performance, leading to a slight artificial step. B: Tilt retrieved after Aoyama and Oshima (2008). While the long-period trend cannot be directly interpreted, each of the 5 events shows a clear tilt on both components. The grey area marks noise caused by the approaching team for retrieval of the instrument. C: Directions and amplitudes of horizontal deformations of the 5 steps, gathered from A and B, showing coinciding directions and roughly consistent ratios of displacement and tilt.

Although one station is not sufficient to fully invert for source locations and/or mechanisms, we explored the potential source space with a forward modeling grid search approach. The displacement field in a homogeneous medium with a free surface, including spatial derivatives (i.e. tilt), can be calculated analytically for various source mechanisms (see Okada, 1992). Using the displacements and tilts observed in the field, we performed a grid search for source locations in a box of 300 x 300 x 100 m^3 around station DY3 (1 m grid spacing). For each of those locations, the source moment was adjusted to match theoretical and observed vertical displacement. We then compared the horizontal displacements of simulation and experiment and discarded locations for which one of the components showed a residual of over 15%. Figure 6.5.10 shows source locations and moments validated with this approach for a 75° dipping normal fault mechanism parallel to the boundary fault inferred by Hjartardóttir et al., 2016. The source is no more than several 10s of metres from the recording station.

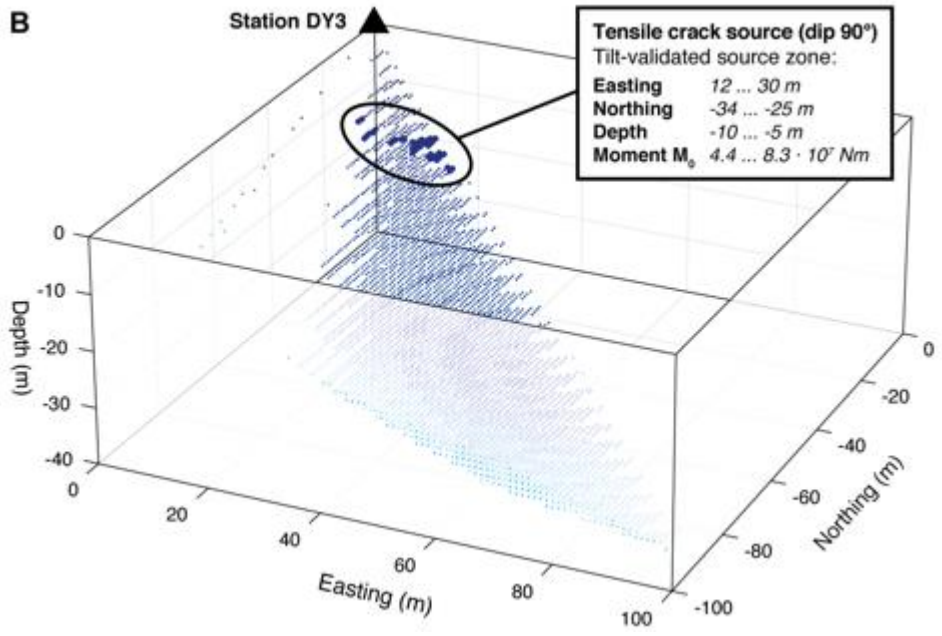

Figure 6.5.10: Source location based on a grid search for combined displacement and tilt. The source is between 35-50 m from recording station DY3.

These novel data and analysis methods give us a unique window into how the dyke is opening at micrometre spatial scale and millisecond temporal scale, based on nearfield observations with a seismometer. Accepting the spatially and temporally limited nature of this unique dataset, it seems that the dyke opens incrementally on the *c*. 5 minute timescale, in 'jumps' of about 100 micrometres, perhaps indicating the 'finest scale' discreteness of the dyke formation process. This raises the question: how do these displacements compare to the observed long-term deformation in the area? Combining the time-history of the closest GPS station with the total graben opening measured from satellite data, the deformation rate for 30 August 2014 is estimated to be roughly 20cm/day. Assuming a repeating process, we extrapolate the steps from our data and obtain a deformation rate of approximately 5 cm/day. Both estimates are very approximate but are of the same order of magnitude. An aseismic component may add to the larger scale deformation, but even if present, cannot be resolved from seismometer displacement data .

Conclusions:

In this deliverable (D6.5) we studied the related topics of seismic tremor and source processes associate with dyke opening/magma migration. The original plan was to address part of the source process work through Moment Tensor (MT) inversion using seismic data. A lack of clear Long Period (LP) data coupled with the unique opportunity to study dyke opening directly in the field during the Holuhraun eruption encouraged us to take a different approach to describing the source. This led to a detailed estimate of the source process and very small spatial and temporal scales. The main points from this deliverable are:

- Seismic waves are significantly distorted by propagation effects in volcanic environments and these path effects must be taken into account when studying seismic sources (beyond fault plane solutions)
- We build a numerical model of the region of interest and use that model to determine path effects, employing full wavefield numerical simulation
- Our understanding of path effects allows us to determine that seismic tremor can be represented by repeating pulses at the source which present as continuous seismic tremor at the recording stations. Synthetic tremor generated using this approach shows excellent visual agreement with field recorded tremor
- A near/above dyke seismic deployment during the Holuhraun eruption has allowed us to see rifting at very small spatial and temporal scales (micrometres & milliseconds). Accepting the spatially and temporally limited nature of this unique dataset, it seems that the dyke opens incrementally on the *c.* 5 minute timescale, in 'jumps' of about 100 micrometres, perhaps indicating the 'finest scale' discreteness of the dyke formation process.
- All envisaged outcomes of this deliverable (D6.5) were achieved or exceeded in terms of our understanding of sources.

Acknowledgements

We are grateful to Martin Möllhoff (UCD), Bergur Bergsson (IMO), Aoife Braiden (UCD) and Heiko Buxel (BGS) for their outstanding contributions in the field. Aoife Braiden for logistics and Martin Möllhoff for seismic data management. Thanks to Andy Hooper and Benni G. Ofeigsson for discussions.

References

Aoyama, H., and H. Oshima (2008), Tilt change recorded by broadband seismometer prior to small phreatic explosion of Meakan-dake volcano, Hokkaido, Japan, *Geophys. Res. Lett.,* 35, L06307, doi:10.1029/2007GL032988*.*

Bean, C.J., I. Lokmer, and G. O'Brien (2008), Influence of near-surface volcanic structure on long-period seismic signals and on moment tensor inversions: Simulated examples from Mount Etna, *J. Geophys. Res.*, 113, B08308, doi:10.1029/2007JB005468.

Bean, C.J. and F. Martini (2010), Sub-basalt seismic imaging using optical-to-acoustic model building and wave-equation-datuming processing, *Marine & Petroleum Geology*, Vol. 27, Issue 2, 555-562 doi:10.1016/j.marpetgeo.2009.09.007.

Darbyshire, F. A., Bjarnason, I. T., White, R. S. & Flovenz, O. G., Crustal structure above the Iceland mantle plume imaged by the ICEMELT refraction profile. *Geophysical Journal International* 135, 1131-1149 (1998)

De Martin, F. Verification of a Spectral-Element Method Code for the Southern California Earthquake Center LOH.3 Viscoelastic Case. *Bull. Seismol. Soc. Am.* **101(6)**, 2855-2865 (2011).

Gardner, G.H.F. L. W. Gardner, A. R. Gregory, Formation velocity and density-the diagnostic basics for stratigraphic traps. *Geophysics* **39(6)**, 770-780 (1974)

Hotovec, A. J., Prejean, S.G, Vidale, J.E & Gomberg, J. Strongly gliding harmonic tremor during the 2009 eruption if Redoubt Volcano. *Journal of Volcanology and Geothermal Research* 259, 89-99 (2013)

Lyons, J. J., G. P. Waite, M. Ichihara, and J. M. Lees (2012), Tilt prior to explosions and the effect of topography on ultra-long-period seismic records at Fuego volcano, Guatemala, *Geophys. Res. Lett.*, 39, L08305, doi:10.1029/2012GL051184.

Martens, H. R. Et al. Dense seismic network provides nw insight into the 2007 Upptyppingar dyke intrusion. Jokull 60,46-66 (2010)
Menke W., West, M., Brandsdottir, B. & Sparks, D. Compressional and shear Velocity structure of the lithosphere in northern Iceland. Bulletin of the *Seismological Society of America* 88, 1561-1571 (1998)

Mitchell, M.A., White, R. S., Roecker, S. & Greenfield, T., Tomographic image of melt storage beneath Askja volcano, Iceland using local microseismicity. *Geophysical Research Letters* 40, 5040-5046 (2013)

Okada, Y. Internal deformation due to shear and tensile faults in a half-space *Bulletin of the Seismological Society of America*, Vol 82, No. 2, 1018-1040, 1992

Palmasson G., Seismic refraction Investigation of the Basalt Lavas in Northern and Eastern Iceland. Jokull 40-47 (1963)

Sigmundsson, F. A. Hooper, S. Hreinsdóttir, K.S. Vogfjörd, B. G. Ófeigsson, E. R. Heimisson, S. Dumont, M. Parks, K. Spaans, G. B. Gudmundsson, V. Drouin, T. Árnadóttir, K. Jónsdóttir, M. T. Gudmundsson, T. Högnadóttir, H. M. Fridriksdóttir, M. Hensch, P. Einarsson, E. Magnússon, S. Samsonov, B. Brandsdóttir, R. S. White, T. Ágústsdóttir, T. Greenfield, R. G. Green, A. R. Hjartardóttir, R. Pedersen, R. A. Bennett, H. Geirsson, P. C. La Femina, H. Björnsson, F. Pálsson, E. Sturkell, C. J. Bean, M. Möllhoff, A. K. Braiden, E. P. S. Eibl, Segmented lateral dyke growth in a rifting event at Bárðarbunga volcanic system, Iceland. *Nature* **517**, 191-195 (2015).

Thun, J., I. Lokmer, and C. J. Bean (2015), New observations of displacement steps associated with volcano seismic long-period events, constrained by step table experiments, Geophys. Res. Lett., 42, 3855-3862, doi: 10.1002/2015GL063924.